

## Article

# Spatiotemporal Patterns of Chlorophyll-*a* Concentration in a Hypersaline Lake Using High Temporal Resolution Remotely Sensed Imagery

R. Douglas Ramsey <sup>1,\*</sup>, Soren M. Brothers <sup>2,3,4</sup>, Melissa Cobo <sup>2</sup> and Wayne A. Wurtsbaugh <sup>2</sup>

<sup>1</sup> Department of Wildland Resources and Ecology Center, Utah State University, Logan, UT 84322, USA

<sup>2</sup> Department of Watershed Sciences and Ecology Center, Utah State University, Logan, UT 84322, USA; sbrothers@rom.on.ca (S.M.B.); melissa@coralrestoration.org (M.C.); wayne.wurtsbaugh@usu.edu (W.A.W.)

<sup>3</sup> Department of Natural History, Royal Ontario Museum, Toronto, ON M5S 2C6, Canada

<sup>4</sup> Department of Ecology and Evolutionary Biology, University of Toronto, Toronto, ON M5S 1A1, Canada

\* Correspondence: doug.ramsey@usu.edu

**Abstract:** The Great Salt Lake (GSL) is the largest saline lake in the Western Hemisphere. It supports billion-dollar industries and recreational activities, and is a vital stopping point for migratory birds. However, little is known about the spatiotemporal variation of phytoplankton biomass in the lake that supports these resources. Spectral reflectance provided by three remote sensing products was compared relative to their relationship with field measurements of chlorophyll *a* (Chl *a*). The MODIS product MCD43A4 with a 500 m spatial resolution provided the best overall ability to map the daily distribution of Chl *a*. The imagery indicated significant spatial variation in Chl *a*, with low concentrations in littoral areas and high concentrations in a nutrient-rich plume coming out of polluted embayment. Seasonal differences in Chl *a* showed higher concentrations in winter but lower in summer due to heavy brine shrimp (*Artemia franciscana*) grazing pressure. Twenty years of imagery revealed a 68% increase in Chl *a*, coinciding with a period of declining lake levels and increasing local human populations, with potentially major implications for the food web and biogeochemical cycling dynamics in the lake. The MCD43A4 daily cloud-free images produced by 16-day temporal composites of MODIS imagery provide a cost-effective and temporally dense means to monitor phytoplankton in the southern (47% surface area) portion of the GSL, but its remaining bays could not be effectively monitored due to shallow depths, and/or plankton with different pigments given extreme hypersaline conditions.

**Keywords:** saline; lake; eutrophication; primary production; MODIS; phytoplankton; *Artemia*



Academic Editor: Teodosio Lacava

Received: 19 November 2024

Revised: 14 January 2025

Accepted: 21 January 2025

Published: 27 January 2025

**Citation:** Ramsey, R.D.; Brothers, S.M.; Cobo, M.; Wurtsbaugh, W.A.

Spatiotemporal Patterns of Chlorophyll-*a* Concentration in a Hypersaline Lake Using High

Temporal Resolution Remotely Sensed Imagery. *Remote Sens.* **2025**, *17*, 430.  
<https://doi.org/10.3390/rs17030430>

**Copyright:** © 2025 by the authors. Licensee MDPI, Basel, Switzerland. This article is an open access article distributed under the terms and conditions of the Creative Commons Attribution (CC BY) license (<https://creativecommons.org/licenses/by/4.0/>).

## 1. Introduction

Phytoplankton production in lakes and oceans is closely associated with chlorophyll-*a* concentration in the water column [1]. Variation and distribution of chlorophyll *a* (Chl *a*) and associated primary production in saline lakes are poorly studied relative to freshwater systems, even though saline lakes represent 44% of the volume of all lakes on Earth [2]. Saline lakes that lack outlets are often nutrient-rich and eutrophic with high chlorophyll concentration and can feature high rates of primary productivity [3]. This high algal productivity supports abundant aquatic invertebrates, making saline lakes critically important for migratory birds [4,5]. The local and continental-scale value of these lakes is underscored by the current global trend in desiccating saline lakes due to anthropogenic water uses [6,7].

One desiccating saline lake of concern is the Great Salt Lake (GSL). It is a highly heterogeneous saline lake in northern Utah, USA, and the largest saline lake in the western hemisphere. Elevations of the GSL have fluctuated since its historic high in 1986 [8], but have steadily decreased over the years, reaching a historic low lake level during the summer of 2022 [9]. The GSL holds significant environmental and economic importance to local and regional interests [10,11]. Industries specific to the lake include mineral extraction, recreation, and harvest of brine shrimp (*Artemia franciscana*) eggs. The lake also provides a suite of ecological services, including extensive wetlands that provide a habitat for millions of migrating waterfowl. The lake's population of brine shrimp and benthic brine flies (*Ephydria gracilis*) provide an important source of food for migrating waterfowl. It is estimated that one-third of all western U.S. migrating waterfowl rely on the GSL as a stop in their migratory path [12], with the majority of the birds migrating to Canada, Mexico, or South America [13], emphasizing the importance of this ecosystem [14]. The brine shrimp population in the GSL is supported primarily by phytoplankton, dominated by a single-celled green alga (*Dunaliella viridis*) and diatoms. Thus, an understanding of temporal fluctuations of phytoplankton within the GSL is critical to the support of ecological and economic benefits that the lake provides.

Traditional methods used to estimate water column Chl *a* concentrations to determine phytoplankton dynamics typically employ point-based sampling from multiple stations dispersed across large lakes and oceans. This methodology provides accurate, point and time-specific data, but is expensive to collect, and often lacks detailed spatial and temporal detail of Chl *a* variability. Remote sensing technologies have long been used to evaluate Chl *a* using space-borne sensors dominated by Landsat's TM, ETM+, OLI, and Terra/Aqua MODIS [15].

In contrast to point-based sampling, satellite imagery provides a holistic view of lakes and oceans at spatial and temporal scales that are impossible to collect in the field. Satellite imagery, however, must be calibrated with field samples using point-based sampling as described above. When calibrated, satellite imagery provides a wholistic view of the phytoplankton distribution across a water body and this distribution can be visualized across time allowing researchers and managers to better understand the factors influencing the distribution and amount of phytoplankton growth across wide areas and multiple time steps [16]. Remote sensing has been used to visualize water column Chl *a* concentrations in fresh and saline lakes since the early days of the Landsat Thematic Mapper instrument [15,17], including Great Salt Lake [18–20].

Here, we test three remote sensing products from space-based platforms to measure Chl *a* concentrations across the GSL. The objectives of this work were to: (1) provide high temporal resolution estimates of the seasonal changes of water column Chl *a* concentrations in the lake throughout the year; (2) investigate if nutrient-rich outflows from hypereutrophic Farmington Bay (Figure 1) influence the spatial distribution of surface Chl *a* concentrations in the largest part of the lake (Gilbert Bay), and; (3) determine if estimating Chl *a* concentration at a long temporal span (20+ years) and high temporal resolution (daily) can improve our understanding of long-term trends in primary production across the GSL, its seasonal variability, and overall changes in phytoplankton dynamics across the 20+ year time span.

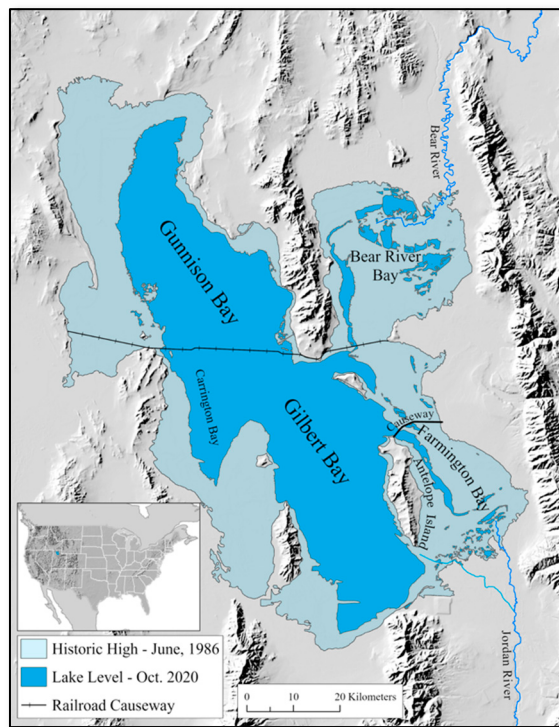


**Figure 1.** The Great Salt Lake in northern Utah, USA, shown at its October 2020 field data collection level. Bear River and Farmington Bays along the eastern side of the lake were extensively desiccated during our field sampling period. The larger light blue area represents the extent of the lake in June of 1986—the historic high. Existing mineral evaporation ponds as well as freshwater impoundments are not included in this map.

## 2. Materials and Methods

### 2.1. Study Area

Great Salt Lake is partitioned into four primary bays: Gilbert, Gunnison, Bear River, and Farmington. The latter two bays were largely dewatered during the period of field sampling for this study (2020–2021, prior to the historic low in the fall of 2022) due to freshwater diversion practices exacerbated by long-term drought. Nearly all inflows to the GSL enter via the Bear River and Farmington Bays. Gunnison and Gilbert Bays are separated by a railroad causeway built in 1959, resulting in the northern Gunnison Bay being significantly more saline than the southern Gilbert Bay as it receives most of its inflow from the already saline Gilbert Bay through a breach or culverts in the causeway [21,22].

Because it is shallow, the surface area of the lake fluctuates significantly with a historic high of 1283.5 m ASL, resulting in a surface area of 5956 km<sup>2</sup> in June 1986. In early November 2022, after years of sustained drought and continuing upstream water diversion, the lake reached a historic low of 1276.7 m ASL, resulting in a surface area of only 34% (2071 km<sup>2</sup>) of the 1986 high. During our field campaigns in 2020 and 2021, Gilbert Bay, our main study area, had respective mean elevations of 1278.2 m and 1277.8 m. The respective mean depths of Gilbert and Gunnison Bays during this period were near 4.6 m and 4.1 m. Morphometric data for Farmington and Bear River Bays are incomplete, but during our campaigns, mean depths for both were <0.3 m. The lake's salinity fluctuates widely, but in 2020 and 2021, Gilbert and Gunnison Bays had respective salinities of 130–150 g L<sup>-1</sup> and 330 g L<sup>-1</sup> (NaCl saturation). Farmington and Bear River Bays are essentially estuaries with freshwater at the inflows and higher salinities near their confluences with Gilbert Bay.

## 2.2. Training Data

In-situ measurements of water column Chl *a* concentrations at specific locations distributed across the Gilbert Bay portion of the GSL were collected across the summer through the fall months of 2006, 2020, and 2021 from three independent field campaigns. Each sample recorded surface Chl *a* concentrations as well as Secchi depth, water depth, longitude and latitude, and date of sample locations.

Field data collected in 2006 consisted of 89 observations from 34 locations sampled on multiple dates spanning May through December [19]. We collected data in 2020–2021 at 45 locations spanning August–October 2020 and April–June 2021 for a total of 98 observations [23]. Finally, data collected by the Great Salt Lake Brine Shrimp Cooperative, Ogden, Utah consisted of 18 observations collected at nine locations once on 26 August 2021, and again on 16 September 2021 (Figure 2). The combined training dataset consisted of 205 observations. Chlorophyll samples collected in 2006 were analyzed by filtering 5–50 mL aliquots through 1  $\mu\text{m}$  Gelman A/E filters and if not analyzed immediately, were frozen at  $-18^{\circ}\text{C}$  for up to two weeks. Chl *a* from the frozen filters was extracted in 10 mL of 95% ethanol for 20–24 h and analyzed with the non-acidification method on a Turner 10AU fluorometer [24]. Chlorophyll samples collected in 2020–2021 were analyzed following the same general protocol followed in 2006 but using 0.45  $\mu\text{m}$  Whatman GF/F filters. Chl *a* samples collected by the Cooperative were also analyzed using standard protocols [25] being concentrated on 0.45  $\mu\text{m}$  M membrane filters and analyzed spectrophotometrically with the acidification method, though we noted that their samples were extracted for 2+ h in 90% acetone. We recognize that their shorter extraction time may result in slightly lower estimates of Chl *a* concentrations than those carried out with our methods, though we considered it likely that this difference would be significant compared to the much broader spatial and temporal variability observed within the lake. We also note that their data points represent less than 5% of the final dataset used for this analysis and so are unlikely to significantly influence results.

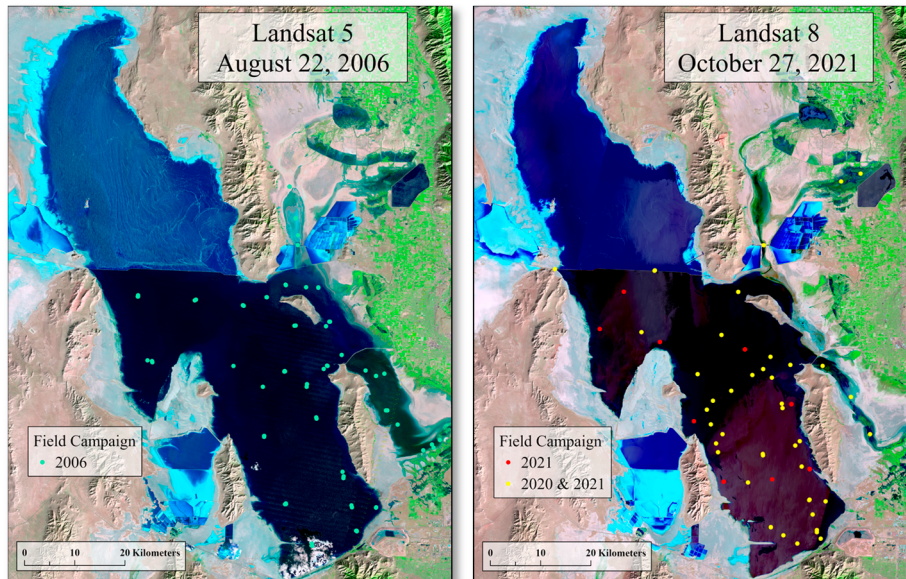


**Figure 2.** In-situ sample sites for 2006 (left) and 2020–2021 (right) field campaigns overlain onto time-relevant Landsat 5 and 8 images. Data for 2021 were provided by the GSL Brine Shrimp Cooperative.

## 2.3. Imagery

MODIS and Landsat image products were compared to assess the strength of the relationship with field-sampled Chl *a* concentration ( $\mu\text{g L}^{-1}$ ) and a derived spectral

index. Landsat 5, 7, and 8 (L5, L7, and L8, respectively), collection 2, level 2, tier 1, 30 m resolution surface reflectance [26] was compared to two MODIS-derived products: MCD43A4 v6.1 daily cloud-free nadir bidirectional reflectance distribution function (BRDF)-adjusted reflectance at 500 m spatial resolution, and MOD09GA v6.1 daily surface reflectance at 500 m resolution. Thus our comparison of three image products consisted of Landsat's 5, 7, and 8 as one product and MODIS MOD09GA and MCD43A4 as the two other products.

The MODIS MCD43A4 daily cloud-free imagery consisted of spectral bands 1–7 at 500 m spatial resolution [27]. This data product was chosen due to its rigorous processing to generate BRDF-adjusted reflectance values as well as its daily cloud-free characteristic generated by employing an 8-day backward and 7-day forward (16 days) lag with the resulting reflectance values weighted toward the 9th day. A potential drawback would be cloud cover in the days bounding the 9th day resulting in reflectance values representing days farther away from the field sample date.

The MODIS MOD09GA data are also a 500 m resolution daily MODIS product corrected to surface reflectance and consisting of spectral bands 1–7. These data represent a single day with no cloud filtering applied [28]. This product was selected due to its processing level to surface reflectance and its daily temporal resolution. The potential downsides include cloud and cloud shadow obscuring sample sites during sampling days.

#### 2.4. Image Processing and Data Extraction

The extraction of reflectance values for each field sample was performed using Google Earth Engine (GEE) [29]. GEE JavaScripts were written to intersect Chl *a* sample locations with images from each of the three remote sensing products filtered by the date of field sample collection. For the MCD43A4 and MOD09GA products, the field sample collection date was used to select images representing only that date. The MOD09GA product was also processed to mask cloud and cloud shadow using its quality assurance layer (“state\_1 km”).

For the Landsat products, the L5, L7, and L8 image collections covering the GSL were merged into a single collection with spectral bands common across the three platforms (bands 1–5, and 7 for L5 and L7, and bands 2–7 for L8) selected and renamed as blue, green, red, NIR, SWIR1, and SWIR2, respectively. This normalized the spectral band name differences between the sensors. To mitigate cloud and cloud shadow, a  $+/- 8$ -day temporal window surrounding the date of field sample collection was used to generate a cloud-free temporal composite. This temporal window accessed a minimum of three images to produce a cloud-free or near-cloud-free composite image. An additional layer representing the per-pixel date of image acquisition was generated and sampled to document the temporal difference between field sample collection and image acquisition date for the corresponding pixel. The intersection of sample points with each of the three image sources produced a data table for each sensor linking field data to reflectance values recorded by each spectral band. The temporal difference between the pixel acquisition and field data collection was also included to assess how this variable affected the correlation between Chl *a* concentration and spectral values.

Quality assurance/quality control was assessed for both spectral and field data. Since several field data collection sites were near shore as well as in shallow water, we were concerned about the overlap of pixels onto dry land—a concern, more acute with the 500 m resolution MODIS imagery. To mitigate this, we examined the spectral response of pixels particularly in the shortwave infrared bands. Spectral reflectance of open water is very predictable but can vary depending on water depth, turbidity, or the presence of suspended chlorophyll. This variation is greater in the visible wavelengths and decreases dramatically in the near and shortwave infrared. The longer wavelengths used by MODIS and Landsat

are thus mostly absorbed at the water surface [30]. Another concern was samples collected in areas of shallow lake depth where benthic vegetation and periphyton (attached algae) are visible from the surface and where the boat propeller may have agitated the lake bottom resulting in abnormal field estimates of Chl *a*.

To identify and remove problematic samples, we first examined spectral response curves for each sample and identified reflectance values in the longest shortwave band (SWIR2) that were abnormally high or even higher compared to the SWIR1 band. We also compared spectral responses in the SWIR2 band with water depth, measured as part of the sampling effort, with the assumption that water absorbs most of this wavelength at the surface. Shallower depths, however, are typically adjacent to dry land, indicating a non-homogeneous pixel composed of both water and dry land. Samples exhibiting abnormally high reflectance in SWIR2 were eliminated, presuming that these pixels were overlapping dry land, or the pixel retained some cloud or cloud shadow pollution. We also compared water depth to the concentration of Chl *a* to determine if samples in shallower water resulted in abnormally high Chl *a* concentration ( $>200 \text{ mg L}^{-1}$ ) [31], thus identifying samples whose Chl *a* concentration may have been influenced by the churning of the lake bottom by the boat propeller. To further address shallow water depth, we examined the change in the coefficient of determination between our spectral index and sampled Chl *a* concentration as samples were systematically removed by increasing water depth. Finally, only samples whose Secchi disk measurements were shallower than total water depth were retained. Samples that met one or more of these criteria were removed from the analysis.

The R statistical software (version 4.3.3; R Core Team, 2024) was used to evaluate linear relationships between the natural log of Chl *a* and spectral indices extracted from each of the three remote sensing datasets. Specifically, the ‘lm’ function from the ‘stats’ package was utilized for linear modeling. A review of the existing literature [15,32–37] provided a number of spectral indices and empirical models used to detect Chl *a* concentrations in fresh and saline lakes. A common thread in this literature relied on various combinations of the visible spectral bands (blue, green, and red). Therefore, we opted to use a simple spectral index: (Blue - Red)/Green [15,32].

Red reflectance is subtracted from blue reflectance to help correct for additional radiance caused by the scattering of non-organic suspended matter [32]. We presume the theory behind this correction is due to the reduced penetration of red light into the water column, thus reducing the scattering effect of suspended particles on blue reflectance, which can penetrate deeper into the water column. For our GSL data, this index produced an inverse relationship with Chl *a* concentration. When we examined the spectral data from MODIS and Landsat, blue reflectance was consistently lower compared to green and red reflectance for higher Chl *a* concentrations at water depths  $< \sim 2 \text{ m}$ . We presume this relationship may be due to a number of factors, including suspended sediments, colored dissolved organic matter (CDOM), and/or Chl *a* fluorescence in the red band [38,39]. Therefore, we altered the published index by inverting the numerator ((Red - Blue)/Green)—henceforth referred to as RBG.

Our results are presented primarily as color-coded images of the entire lake, with an emphasis on Gilbert Bay, where our training data were obtained. However, to emphasize spatial and temporal trends in the data, chlorophyll concentrations from pixels located at three in-situ sampling stations (GB 14, GB 3510, and GB4069), and two other sites (Plume area and Carrington Bay), were composited from the 20-year MODIS imagery. These sites show the variability in chlorophyll concentrations in Gilbert Bay.

### 3. Results

#### 3.1. Satellite Product Comparisons

Our comparison between field measurements of Chl  $a$  concentration and the RBG spectral index extracted from Landsat and the two MODIS products showed that the index derived from the MODIS MCD43A4 product provided the overall strongest relationship with the natural log of Chl  $a$  concentration ( $\mu\text{g L}^{-1}$ ). Landsat surface reflectance values correlated against the natural log of Chl  $a$  resulted in an  $R^2$  of 0.465 ( $n = 99, p < 0.00$ ). The MOD09GA product provided an  $R^2$  of 0.742 ( $n = 33, p < 0.00$ ), and the MCD43A4 product resulted in an  $R^2$  of 0.726 ( $n = 100, p < 0.00$ )

The relationship between Landsat-derived RBG and Chl  $a$  concentration resulted in the lowest  $R^2$  (0.465), primarily due to the variable temporal difference between the field measurement of Chl  $a$  and an available cloud-free pixel. This temporal variation spanned 0 to 8 days. When the sampled pixel was collected on the same day as the field sample, the correlation coefficient between Landsat and Chl  $a$  concentration increased to 0.836, but with a very low sample size ( $n = 15$ ). As the temporal distance between the pixel and sample point increased to over 1 day, the correlation coefficient dropped incrementally to 0.465 as the day distance increased.

Both MODIS products resulted in similar  $R^2$  values. However, the MCD43A4 product had significantly more usable samples compared to MOD09GA (100 vs. 33). This was due to the significantly higher number of samples lost to cloud cover in the MOD09GA product. Thus, the daily cloud-free frequency of the MCD43A4 product and greater confidence due to sample size was considered superior to MOD09GA for the purposes of this study.

Eliminating samples in the shallowest regions of the lake (<0.55 m water depth) improved the correlation with our field measurements of Chl  $a$ . Figure 3 shows the relationship between water depth and reflectance in the shortwave infrared band SWIR2 (2105–2155 nm) from MODIS (Figure 3A), the relationship between water depth and Chl  $a$  concentration (Figure 3B), and the changes in the coefficient of determination ( $R^2$ ) and sample size as samples with shallower water depths were systematically eliminated (Figure 3C). Reflectance in the SWIR2 band averaged 0.57% ( $SD = 0.44$ ) for pixels sampled in water deeper than 0.55 m (relative open water). However, as water depth decreased below 0.55 m, average SWIR2 reflectance increased to 1.78% ( $SD = 2.66$ ). Reflectance in SWIR2 increased in shallow water for the sampled 500 m<sup>2</sup> MODIS pixels, likely due to overlap with adjacent land. Furthermore, for some samples, the relationship between water depth and measured Chl  $a$  concentration may have been influenced by disturbance of benthic substrate by the airboat, which put periphyton and/or settled phytoplankton into the water column (despite efforts to minimize this effect during sampling). The  $R^2$  between the RBG index and measured Chl  $a$  concentration as water depth increases was variable from 0 to 0.55 m, and then remained relatively stable. The sample size, however, decreased significantly as we deleted samples whose water depth was >0.55 m. We therefore excluded data collected at depths less than 0.55 m.

Eliminating field samples using the criteria defined in the Methods Section resulted in a cleaner, more realistic, set of spectral signatures for each sample (Figure 4). In general, the spectral signatures of samples that were removed showed higher spectral reflectance in the NIR and SWIR bands, which is uncharacteristic of water surfaces. Many of these sites were located nearshore, where the 500 m spatial resolution of the MODIS imagery could have included patches of dry land. These sites may also have been polluted with residual clouds present in the MODIS or Landsat imagery.

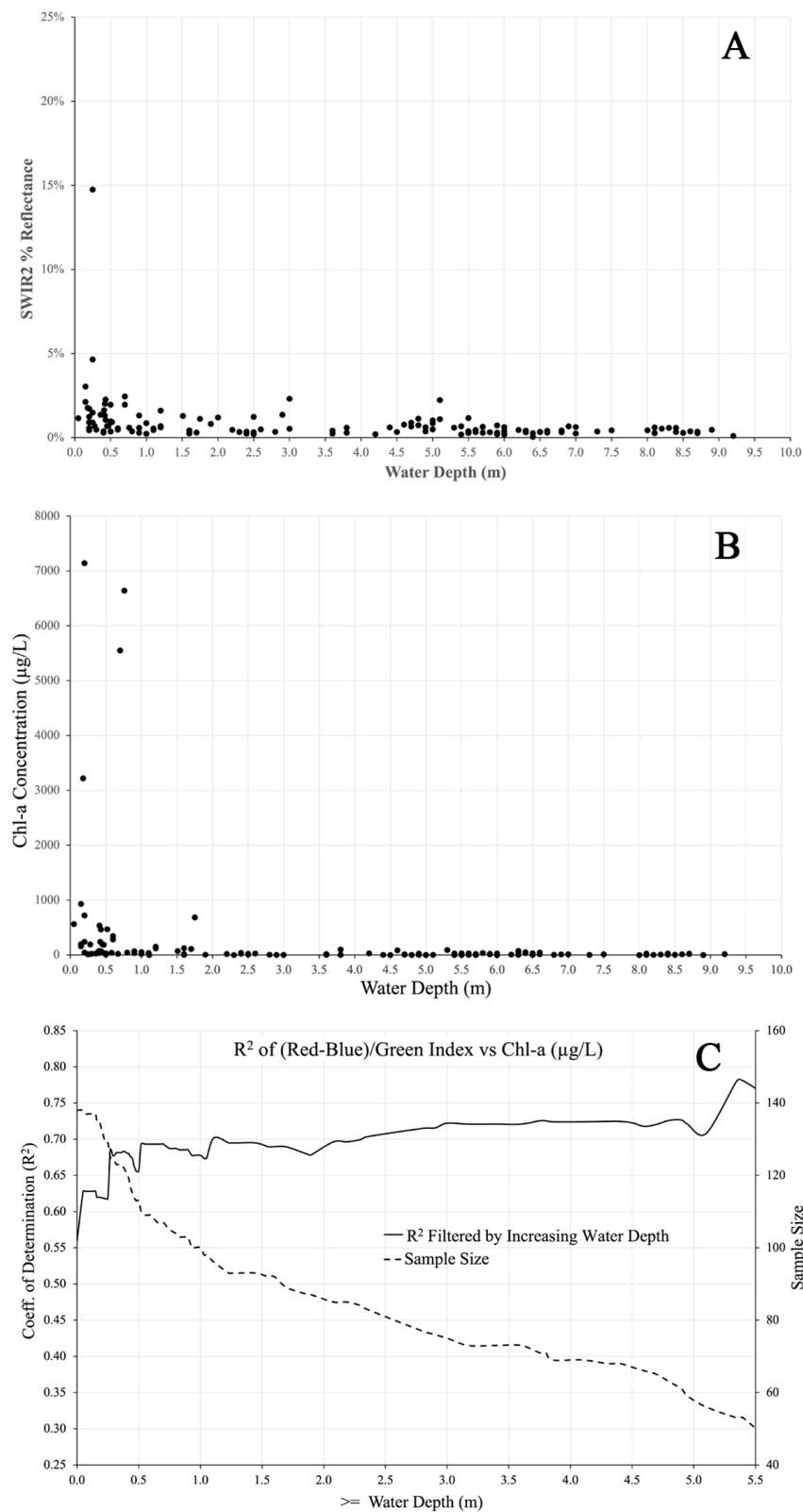


**Figure 3.** (A) Relationship between water depth and spectral reflectance in the MODIS SWIR2 band. (B) Relationship between water depth and field-measured Chl  $a$  concentration. (C) Change in the Coefficient of Determination between the RBG index and field-measured Chl  $a$  concentration as shallower water depths are eliminated.

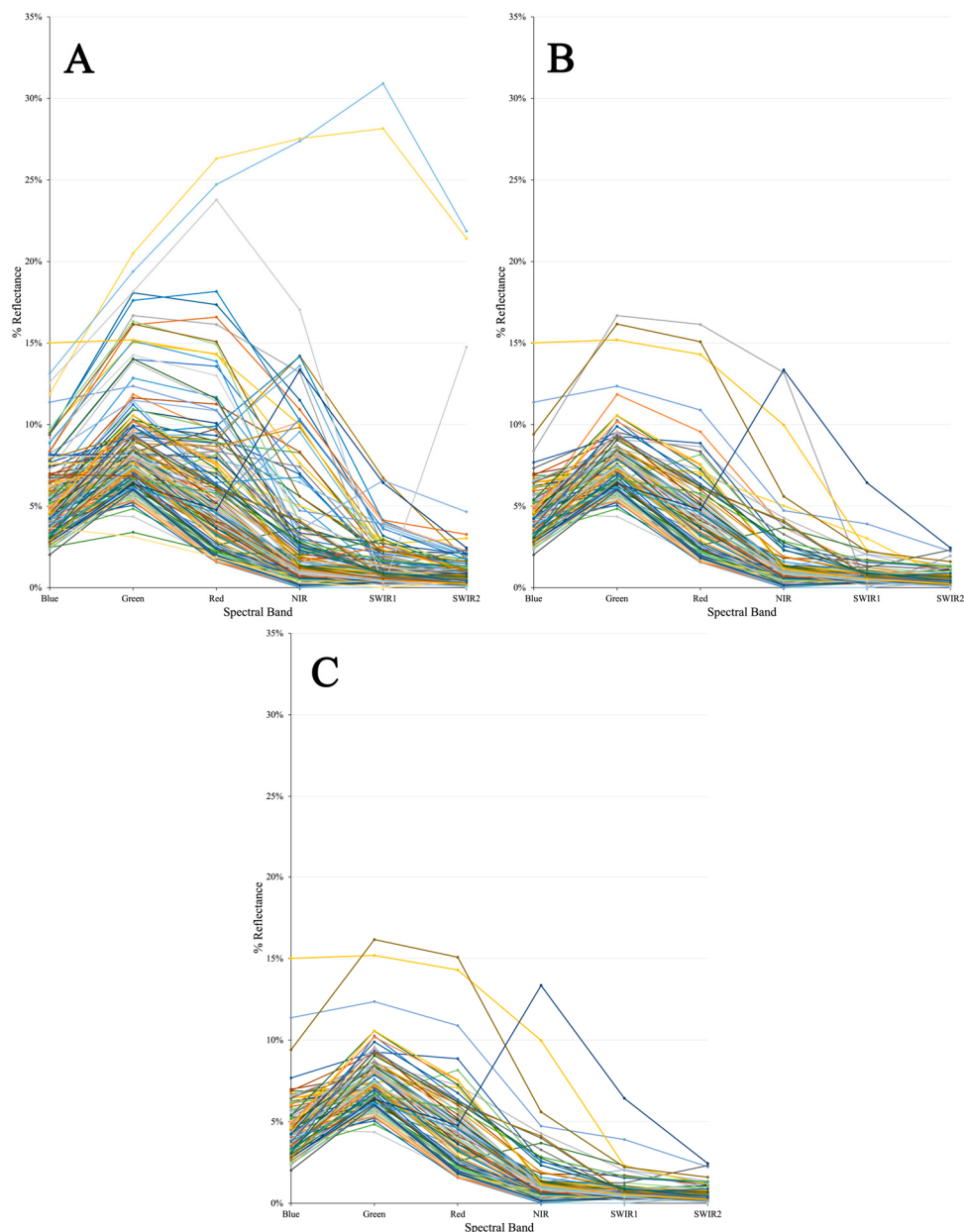


**Figure 4.** Spectral signature plots of sampling sites recovered from the MCD43A4 MODIS product. (A) Spectral signatures of all samples. Higher reflectance in the near and shortwave IR exhibits abnormal water responses and is more consistent with shallow/muddy water, land, or possibly clouds. (B) Spectral signatures of sampling sites where water depths  $\geq 0.55$  m. (C) Spectral signatures of samples where water depths  $\geq 0.55$  m and Chl  $a$  concentration  $\leq 200 \mu\text{g L}^{-1}$ . Line colors are only used to help differentiate signatures.

### 3.2. Spatial-Temporal Variation in Chlorophyll

Figure 5 shows the relationship used to predict per-pixel Chl  $a$  concentrations across the GSL using the relationship between the MCD43A4-derived RBG index and  $\log^{10}$  Chl  $a$  concentrations. A 25x cross-validation of the correlation between the natural log of Chl  $a$  and the RBG index derived from the MCD43A4 was performed by randomly sub-setting the 100 samples used in Figure 5 into a 70%/30% split of training and validation points, respectively. The average  $R^2$  values for training and validation sets were 0.7280 and 0.7290, with standard deviations of 0.0287 and 0.0651, respectively.

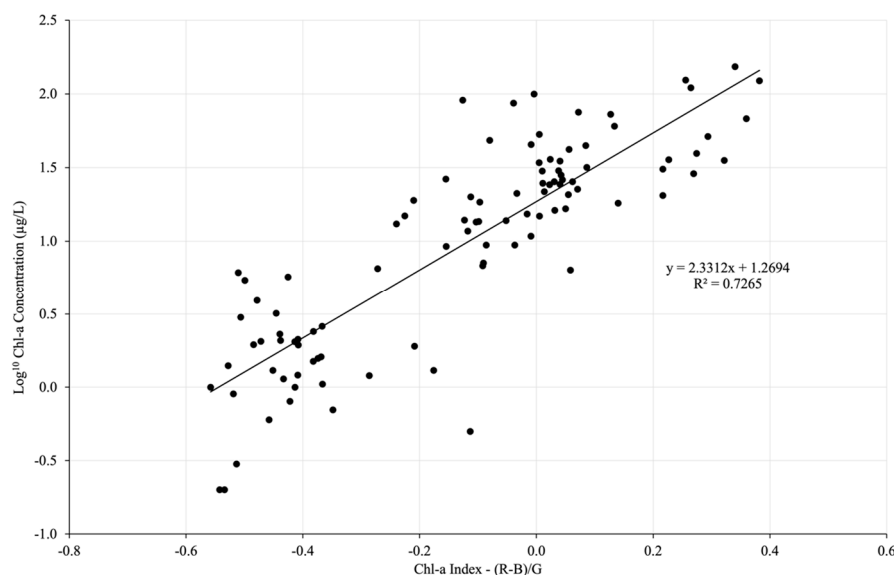


**Figure 5.** Relationship between the RBG index from the MCD43A4 MODIS imagery and Log<sub>10</sub> Chl *a* concentrations from field collections. Sample points include only those samples where water depth was  $\geq 0.55$  m and field-based Chl *a* measurement was  $\leq 200 \mu\text{g L}^{-1}$ .

The remote sensing model results for Farmington, Bear River, and Gunnison Bays almost always showed very high Chl *a* concentrations ( $50$ – $200 \mu\text{g L}^{-1}$ ) (Figure 6). These high concentrations may be erroneous due to the lack of valid sampling sites in those areas as a result of shallow water and the coarse spatial resolution of the MCD43A4 product (500 m), which overlapped onto dry land in these shallow areas. Although high Chl *a* concentrations were measured in the water column samples in these bays (as discussed below), for the remote sensing analysis, we considered these concentrations to likely be artifacts. At the current low level of the GSL, water depths in Farmington and Bear River Bays are  $<0.50$  m in most locations, so it is likely that the satellite imagery recorded periphyton on the bottom, or aquatic macrophytes that often reach the surface, particularly in the eastern portion of Bear River Bay, commonly known as the Willard Spur. Nevertheless, Farmington Bay, and to a lesser extent Bear River Bay, are highly productive with generally high concentrations of phytoplankton [40], so the plots in Figure 6 may fortuitously show realistic concentrations. The high concentrations of Chl *a* depicted in Gunnison Bay (Figures 6 and 7), however, are unreliable because insufficient field samples were available in that bay to calibrate the remote sensing imagery. The hypersaline Gunnison Bay contains a different microbial community compared to Gilbert Bay [41], producing a very different spectral reflectance, as noted by the color difference depicted in the 22 August 2006 Landsat image in Figure 2.

MODIS imagery for Gilbert Bay on individual dates often showed distinct spatial patterns of chlorophyll in the lake. For instance, on 15 November 2020 (Figure 6), there is a plume extending out from the Farmington Bay outflow near the northern tip of Antelope Island and into the northern part of Gilbert Bay. When we averaged multiple consecutive dates to obtain mean bi-monthly patterns (Figure 7), detailed patterns were lost, but there was still marked spatial-temporal seasonal variation within Gilbert Bay.

Curiously, the shallower margins of the lake sometimes had lower Chl *a* concentration compared to open water, and this was evident in the November/December 2020 Chl *a* average (Figure 7F). In the March-April summary (Figure 7B), Chl *a* concentrations were higher in the northern portion of Gilbert Bay and there is some evidence of a plume driven by nutrients coming out of Farmington Bay. From May-August (Figure 7C,D), when brine shrimp are abundant, Chl *a* concentrations were mostly  $<3 \mu\text{g L}^{-1}$ , and there was no

evidence of a plume coming out of Farmington Bay. In areas where microbialites are abundant along the margins of the lake, the imagery suggests higher Chl *a* concentrations, but this may be an artifact of reflectance from the periphyton on these structures and not phytoplankton in the water column. In the fall and early winter of 2020 (Figure 7E,F), Chl *a* concentrations in Gilbert Bay increased considerably, but concentrations were generally lower in Carrington Bay (the northwestern portion of Gilbert Bay) than in the rest of the bay. In the November and December plots (Figure 7F), there was again evidence of a plume driven by the nutrient-rich water coming out of Farmington Bay. An animated GIF depicting the daily changes in spatial concentrations of Chl *a* in the lake during 2020 is available here and demonstrates the rapid spatial-temporal changes that can occur in the lake.

The seasonal cycles of Chl *a* concentrations for the three sites in the southern (GSL 4069), central (Plume), and Carrington areas of Gilbert Bay for four years (2018–2021) are shown in Figure 8 (site locations are shown in Appendix A as Figure A1.) Chlorophyll concentrations in winter were generally 20–60  $\mu\text{g L}^{-1}$  but decreased to <5  $\mu\text{g L}^{-1}$  in late spring and summer, then increased through the fall. The three sites showed generally similar yearly patterns with apparent high weekly variability. Seasonal cycles of Chl *a*, derived from MCD43A4 spanning 20 years for 14 stations, can be found in the Excel file—DailyStationData\_MCD43A4.xlsx.

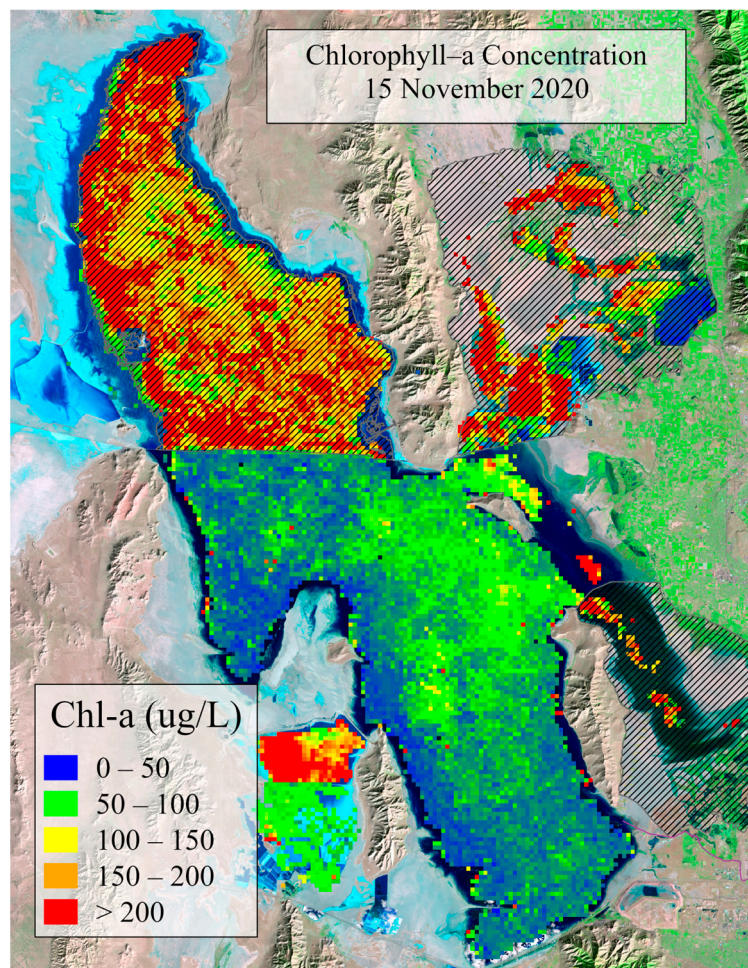


**Figure 6.** Spatial pattern of chlorophyll in Great Salt Lake on 15 November 2020, determined using MODIS satellite imagery. Concentrations depicted in Farmington, Bear River Bay, and Gunnison Bay and the large salt evaporator to the southwest (hashed areas) may be erroneous (see text). Also, note the presence of solar salt ponds in the SW of Gilbert Bay and the SE part of Bear River Bay.

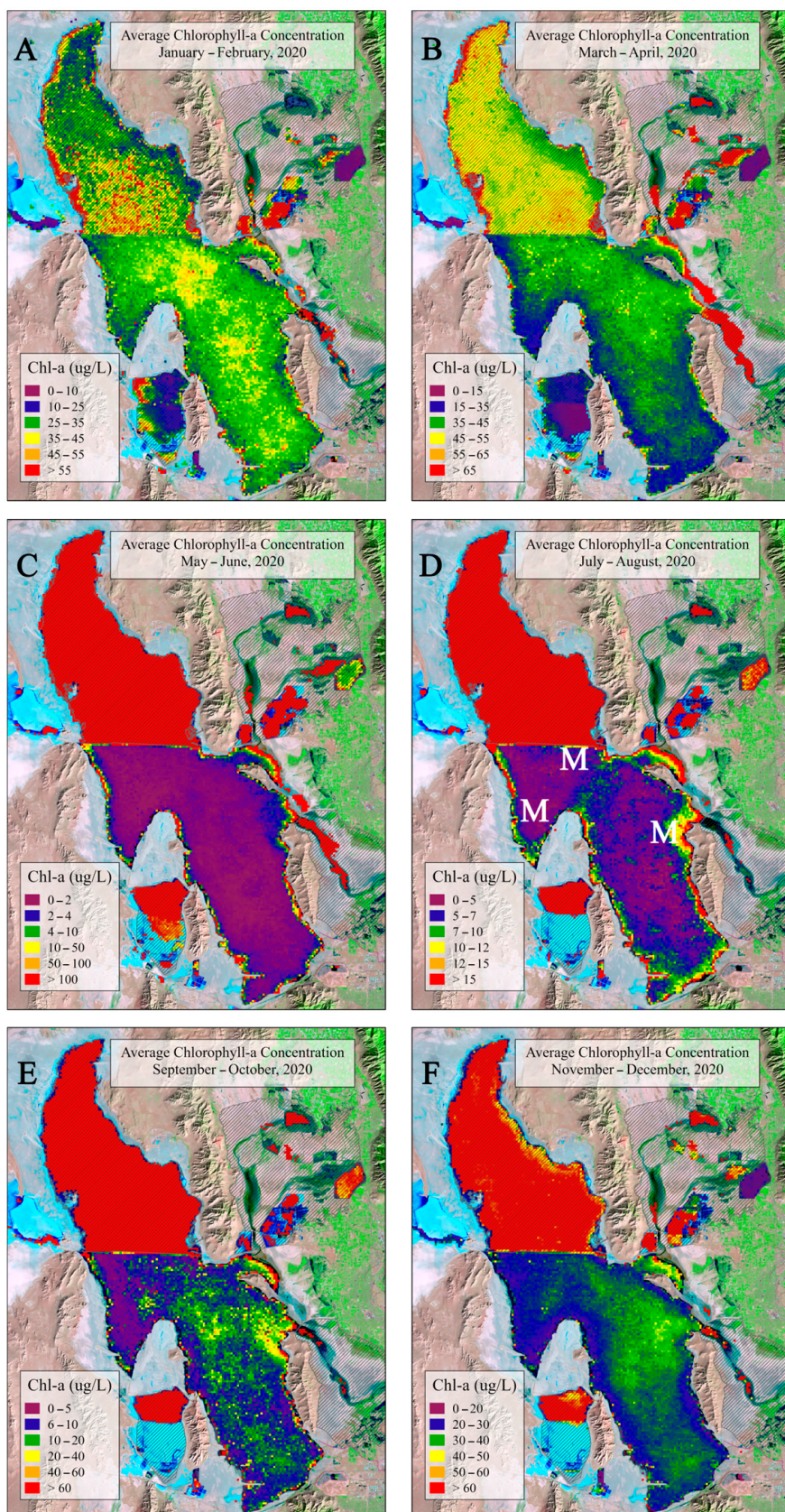


**Figure 7.** Bi-monthly (A–F) mean pelagic chlorophyll levels in GSL in 2020. Each mean was calculated from 60–61 daily images (2 months) from the MODIS satellite. Note the different color scales in the different frames. When chlorophyll levels were low from May–August (C,D), the lake clarity would have been high, allowing for periphyton along the lake perimeter and on microbialite fields (noted with

“M” in the July–August plot (D); NW of Antelope Is., Ogden Bay, Carrington Bay, and south end of Gilbert Bay) to over-estimate Chl  $a$  in the plankton. Similarly, in shallow Farmington and Bear River Bays (NE and SE hashed areas), phytoplankton Chl  $a$  concentrations were likely overestimated, although these bays are highly productive. Concentrations in Gunnison Bay (hashed area above the railroad causeway) are not reliable, as the satellite imagery was not calibrated for the unusual microbial pigments there.

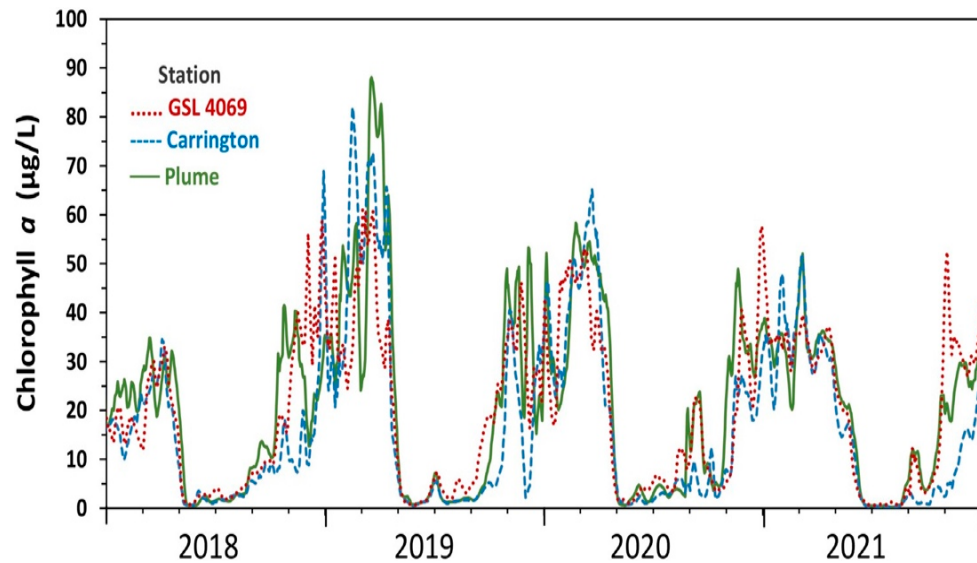


**Figure 8.** Annual cycles in Chl  $a$  concentrations at three stations sites in Gilbert Bay over four years, determined by satellite imagery. Locations of the pixels used for this analysis are shown in Figure A1. These three sites were chosen because they potentially represent the most diverse sites in Gilbert Bay. Lines are 7-point running means to provide smoothing.

A summary of the seasonal cycle in Chl  $a$  averaged over 20 years (2001–2021) and *Artemia* abundances from 1996–2004 [31,42] (Figure 9) shows that Chl  $a$  concentrations peak in March at approximately  $37 \mu\text{g L}^{-1}$  and then decline to  $3 \mu\text{g L}^{-1}$  by June, presumably due to strong grazing pressure by *Artemia*, which increases in population in the early summer months. With mean adult-equivalent densities of  $3 \text{ L}^{-1}$  in summer, *Artemia* can consume approximately 72% of the phytoplankton in the water column each day [43]. Mean chlorophyll concentrations increase to  $23 \mu\text{g L}^{-1}$  by November when cooler temperatures result in a winter die-off of *Artemia*, thus reducing grazing pressure.

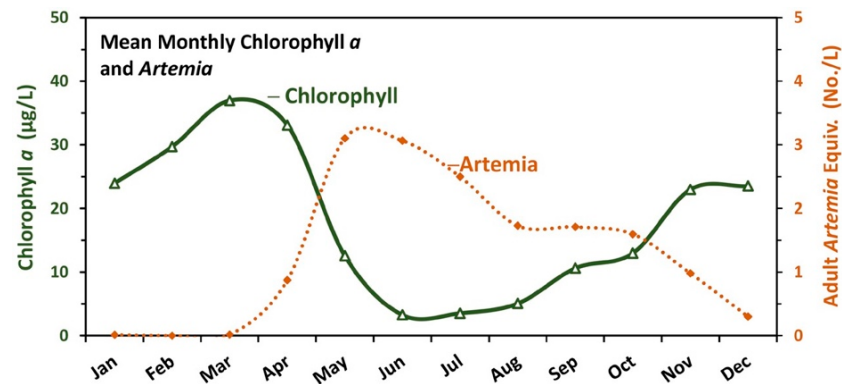


**Figure 9.** Mean monthly Chl  $a$  concentrations at five open-lake locations in Gilbert Bay, estimated by satellite imagery from 2001 to 2021. The Artemia curve shows mean adult equivalents from 1996 to 2004, based on data from [44].

Mean annual Chl  $a$  concentrations in Gilbert Bay ranged from 10 to over 30  $\mu\text{g L}^{-1}$  over the 2001–2021 period, when two additional sites in Gilbert Bay (GB14 and GSL3510) (Figure A1) were included with the three aforementioned sites. Each of the five sites had similar temporal patterns of Chl  $a$  concentrations over time. Concentrations were significantly lower (2-way ANOVA;  $p < 0.001$ ) at the Carrington Bay station by 14% compared to the other four stations in Gilbert Bay, which had remarkably similar mean Chl  $a$  concentrations to one another. This 20-year analysis of the MCD43A4 MODIS imagery indicated that overall mean annual Chl  $a$  concentrations in Gilbert Bay have increased significantly ( $p = 0.014$ ) from approximately 14  $\mu\text{g L}^{-1}$  to 23  $\mu\text{g L}^{-1}$  (Figure 10b).

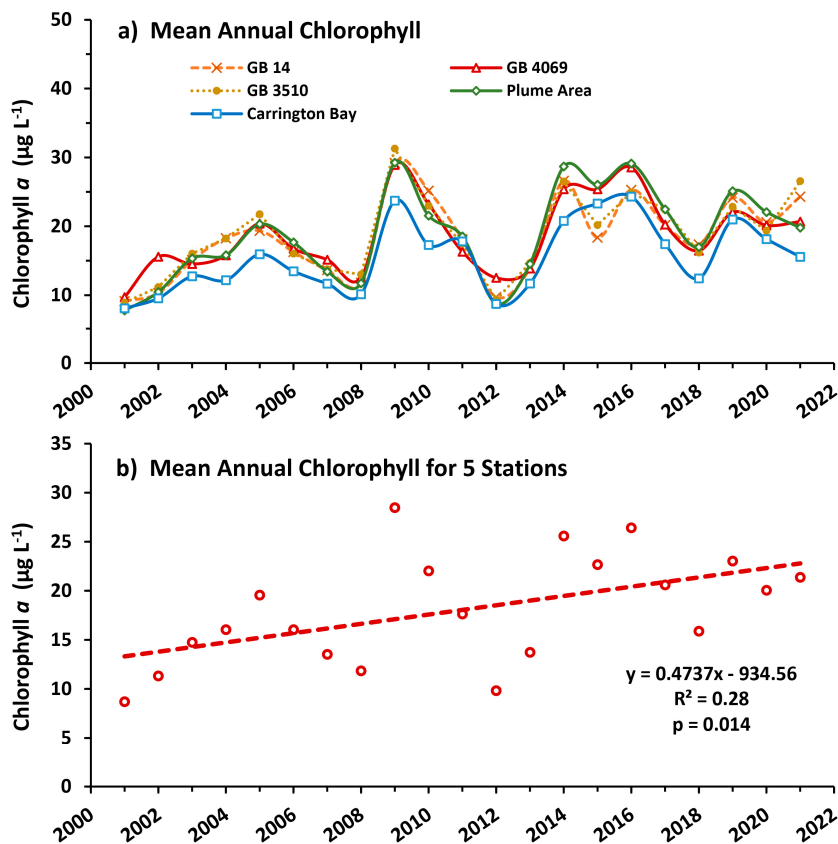


**Figure 10.** Mean chlorophyll levels in Great Salt Lake between 2001 and 2021, measured by satellite imagery. (a) Chl  $a$  concentrations at five open-lake stations in Gilbert Bay. (b) Mean concentrations of the five stations from 2001 to 2021.

## 4. Discussion

### 4.1. Remote Sensing

Of the three remote sensing products that we tested, we concluded that MCD43A4 provided the best overall relationship with Chl  $a$  due to its daily cloud-free characteristic. This product is generated by employing an 8-day backward and 7-day forward lag, with the resulting reflectance values weighted toward the 9th day. This ostensibly resulted in spectral reflectance for a given pixel recorded on, or adjacent to the date of field data collection. This is supported by our analysis of Landsat reflectance values, which were filtered to include only those that were collected on the same day as field data collection. This resulted in the highest correlation ( $r^2 = 0.836$ ) but decimated our samples to only 15. As the temporal difference between Landsat image collection date and field sample date increased, the relationship quickly collapsed. Water currents that constantly move Chl  $a$  across the lake compromise the spatio-temporal relationship between the remote sensing instruments and their targets [20,45,46]. The MODIS MOD09GA product provides daily

reflectance since this dataset is not a result of fusing temporally sequential images, thus minimizing the temporal disparity with field samples. The results between MOD09GA and MCD43A4 were similar, with MOD09GA performing slightly better, however, cloud pollution in the MOD09GA product decimated the sample size ( $n = 33$ ) compared to MCD43A4. We, therefore, concluded that the MCD43A4 product was superior to MOD09GA where this study is concerned since it allowed us to map the distribution and concentration of Chl *a* on a daily basis, spanning February 2000 to October 2022, without the need to account for cloud effects.

#### 4.2. Spatial-Temporal Changes in Chlorophyll

##### 4.2.1. Broad Scale Patterns in Gilbert Bay

The MCD43A4 MODIS imagery provided excellent insights into the spatio-temporal changes of Chl *a* in Gilbert Bay. Individual images showed highly varied patterns in the lake, but bi-monthly averages showed general patterns indicative of the mixing that occurs in this wind-swept lake. Three general patterns and insights were evident. First, the western portion of the lake, Carrington Bay, usually had lower Chl *a* concentrations than the rest of the lake (14% less, on average). This is likely the result of the bay being distant from the riverine nutrient inputs entering on the east side of the lake. Additionally, Carrington Bay may, at times, have separate gyres from the eastern portion of Gilbert Bay [47], as supported by our video of Chl *a* concentrations.

A second unexpected result from the remote sensing data was the lower Chl *a* concentrations around the shallow perimeter of the lake in winter (Figure 7). This may possibly be due to colder winter temperatures in the shallower water [48]. Additionally, the high chlorophyll concentrations in winter and lower concentrations in summer may not directly reflect rates of primary production, as the grazed populations in summer may feature proportionately higher production rates than the phytoplankton in winter in the absence of grazing [49], and cold temperatures can substantially suppress phytoplankton production rates when light is not limiting [50]. Nevertheless, the rich over-wintering phytoplankton biomass may play an important ecological role in annual lake food web dynamics, promoting rapid growth of *Artemia* in spring (Figure 9) [31] and thus food for migratory birds as well.

A third insight gained from this work is that there is, at times, a nutrient-rich plume coming out of Farmington Bay that supports phytoplankton growth. Approximately 50% of the inflow to Farmington Bay is secondary-treated wastewater with very high nutrient (phosphorus and nitrogen) concentrations (L. Meyers, Central Davis Sewer District, *pers. comm.*). Outflows from Farmington Bay have been estimated to contribute 45% of the nitrogen loading to Gilbert Bay, where nitrogen is the limiting nutrient for phytoplankton growth [51–54]. The relative contribution of nutrient loading from Farmington Bay is small in the spring when the larger Bear River is dominant, but important in the summer and fall [19]. In contrast to the observed plumes coming out of Farmington, the long-term mean Chl *a* concentrations at the Plume Station were not higher than in other parts of the eastern section of Gilbert Bay (Figure 10). Consequently, the importance of Farmington Bay as a nutrient source for Gilbert Bay is unclear. A 2010 detailed study of the plume from Farmington Bay indicated that most indices of enrichment were gone within 3–7 km from the bridge discharge into Gilbert Bay [55]. Although satellite imagery showed important contributions of nutrients from Farmington Bay, a more thorough analysis of the lake's nutrient budget is needed to determine the overall importance of different sources. Imagery did not show plumes coming out of Bear River Bay, which may have been a consequence of the severe drought, particularly in 2021, when Bear River discharges were unusually

low, and lower population densities in the northern part of the state that would generate secondary-treated nutrient rich inflow.

#### 4.2.2. Temporal Changes in Chl *a*

Seasonal changes in Chl *a* were marked. Mean winter chlorophyll concentrations over  $30 \mu\text{g L}^{-1}$  indicate that Gilbert Bay is eutrophic [56]. These high chlorophyll concentrations are possible because *Artemia* is absent and the population of protozoan grazers is not effective in removing phytoplankton in winter [57]. However, mean winter lake temperatures in Gilbert Bay are only  $4^\circ\text{C}$ , whereas in summer they average  $24^\circ\text{C}$  [31], and the cold temperatures may potentially slow production independently of the phytoplankton biomass present. In summer, warm temperatures allow high densities of *Artemia* to decrease phytoplankton Chl *a* to oligotrophic levels. This strong top-down control [43] is facilitated in the hypersaline basins of this lake because there are no fish predators, thus allowing for high densities of the large, highly effective *Artemia* grazers.

The significant increase (68%) in water column Chl *a* in Gilbert Bay in the past 20 years (Figure 10b) indicates a marked increase in the lake's phytoplankton productivity. A model [58] suggests that densities of *Dunaliella*, the dominant species of phytoplankton in Gilbert Bay, should have decreased with increases in salinity as lake levels decreased ( $90 \rightarrow 150 \text{ g L}^{-1}$ ) over the past 20 years, but we found that chlorophyll levels were not correlated with salinity in Gilbert Bay during the 20-year period ( $r^2 = 0.053, p = 0.317$ ). However, the 68% increase in chlorophyll indicates that other factors must be important. Paleolimnological analyses of cores from Gilbert Bay [59] and Farmington Bay [60] also indicate long-term increases in phytoplankton productivity. This may be the result of both decreasing water volumes (due to freshwater diversions, primarily for agriculture [7]) and increased nutrient loading in the watershed associated with a human population increase of 44% (2.02 to 2.93 million) over the 20-year span. Fluctuations in saline lake levels can have major impacts on algal abundance [61], and the GSL has in this period experienced a lake elevation decline of 2.6 m, losing 40% of its volume [9]. Chlorophyll levels in Gilbert Bay were highly correlated with lake level over this period ( $r^2 = 0.518, p = 0.014$ ). While increasing Chl *a* concentrations are relatively rare in lakes across the U.S. West [52], paleolimnological analyses of Utah Lake (directly to the south of, and feeding into, the GSL) have identified nutrient loading from wastewater treatment plants as a major driver of recent eutrophication in that system [62].

Another possible interacting factor that may have increased nutrients available to phytoplankton is erosion of the deep brine layer as the lake decreased in elevation by 2.6 m from 1280.0 m to 1277.5 over the 20-year span. The deep brine layer sequesters nutrients and has ammonium concentrations over  $8 \text{ mg N L}^{-1}$  and nearly 10 times the total N of that in the upper mixed layer [63]. The mixed layer of the lake maintains a relatively constant thickness of 6 m due to wind action, so as the lake level declines, the deep brine layer is eroded. Based on morphometry [9], the 2.6 m decrease would have decreased the volume of the deep brine layer by 93% and greatly reduced the sequestration of nutrient particles sedimenting into it [64], thus enhancing the overall primary productivity. This hypothesis is supported by observations made at the saline Mono Lake in California, where there was a strong negative correlation between lake elevation and chlorophyll concentrations, and a large increase in algal primary productivity after the breakdown of meromixis [65].

Unlike many systems [66], the increasing eutrophication of Gilbert Bay is not necessarily bad. Both experimental [54] and field studies [31,65] have shown that increasing phytoplankton increases the production of *Artemia* that supports millions of birds that migrate to the lake to feed and raise young [67]. Additionally, the harvest of the resting eggs (cysts) of *Artemia* supports a \$US 70 million dollar aquaculture industry [68]. Al-

though Gilbert Bay may benefit from the nutrient loading, the impact on hypereutrophic Farmington Bay is controversial. The extreme cyanotoxin levels there could limit recreation and harm bird populations [40], but the extreme nutrient loading also supports high invertebrate and bird populations [69,70].

## 5. Conclusions

We demonstrated that remote sensing techniques can reveal valuable limnological insights into long-term, seasonal, and spatial trends in large systems that can otherwise pose multiple challenges for sampling-based studies. We identified limitations in the remote sensing approach, including nearshore shallow and extreme hypersaline zones that needed to be excluded due to water depth impacting field sample quality and pixels overlapping dry land. We showed that the temporal separation between image collection and field sample collection dates significantly impacts the relationship between the two and that same-day or near same-day image/field data collection is ideal. Imagery collected by the MODIS/MCD43A4 product provided daily estimates of Chl *a* concentration and distribution across the lake from 2000 to the present, demonstrating that the GSL phytoplankton dynamics feature recurrent seasonal and spatial patterns across the lake as well as a long-term increase in recent decades. Together, these observations provide key knowledge for future studies that investigate the biogeochemical and food web implications of these trends, while also providing lake management agencies, local industry, and other stakeholders with potentially valuable information to ensure the future conditions of the lake are maintained for the mutual benefit of its ecosystem and society.

**Author Contributions:** R.D.R. contributed to the data curation, formal analysis, and methodology of remotely sensed imagery, as well as original draft preparation; S.M.B. contributed to the conceptualization, field data curation, formal analysis, funding acquisition, investigation, field methodology, resources, supervision, and manuscript writing (review and editing); M.C. contributed to field data collection and reviewing and editing the manuscript; W.A.W. contributed to the conceptualization, formal analysis, field investigation, field methodology, resources, and manuscript writing (review and editing). All authors have read and agreed to the published version of the manuscript.

**Funding:** This work was partially supported by a grant from the Utah Division of Forestry, Fire, and State Lands. The funding agency had no role in the study design, collection, analysis, or interpretation of data, writing of the report, or submitting the article for publication.

**Data Availability Statement:** Spreadsheets used to analyze our data are stored in a GitHub repository at <https://github.com/RDRamsey/GSL/tree/main>, accessed on 15 November 2024. This repository contains Excel spreadsheets of field-measured Chl *a* concentration vs. spectral data for the three image products used as well as modeled data for seasonal cycles of Chl *a* derived from MCD43A4 spanning 20 years for 14 stations.

**Acknowledgments:** Dave Naftz, Shane Brandt, and Phil Brown of the Great Salt Lake Brine Shrimp Cooperative helped with the acquisition of chlorophyll data from the lake. We thank Benjamin Brown, Alexander Anderson, and Marshall Baillie at the Utah Division of Water Quality for airboat sampling support, Christine Rumsey and Ryan Rowland from the United States Geological Survey for logistical support and sampling on Gilbert Bay, and Maycee Page and Rachel Chamberlain for assistance in the field and lab work.

**Conflicts of Interest:** The authors declare no conflicts of interest. The funders had no role in the design of this study; in the collection, analyses, or interpretation of data; in the writing of this manuscript; or in the decision to publish the results.

## Appendix A

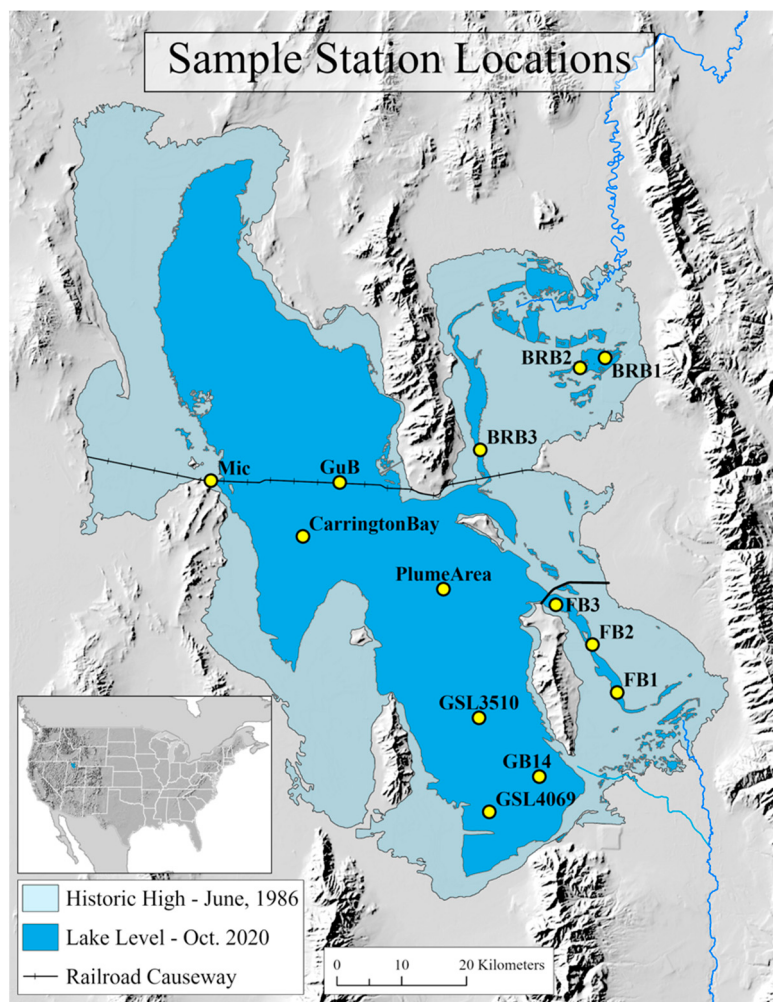


**Figure A1.** Location of 14 sampling stations.

## References

1. Huot, Y.; Babin, M.; Bruyant, F.; Grob, C.; Twardowski, M.S.; Claustre, H. Does Chlorophyll a Provide the Best Index of Phytoplankton Biomass for Primary Productivity Studies? *Biogeosci. Discuss.* **2007**, *4*, 707–745.
2. Messager, M.L.; Lehner, B.; Grill, G.; Nedeva, I.; Schmitt, O. Estimating the Volume and Age of Water Stored in Global Lakes Using a Geo-Statistical Approach. *Nat. Commun.* **2016**, *7*, 13603. [CrossRef] [PubMed]
3. Hammer, U.T. Primary Production in Saline Lakes. *Hydrobiologia* **1981**, *81*, 47–57. [CrossRef]
4. Timms, B.V. Waterbirds of the Saline Lakes of the Paroo, Arid-Zone Australia: A Review with Special Reference to Diversity and Conservation. *Nat. Resour. Environ.* **2009**, *15*, 46.
5. Roberts, A.J. Avian Diets in a Saline Ecosystem: Great Salt Lake, Utah, USA. *Hum.-Wildl. Interact.* **2013**, *7*, 158–168. [CrossRef]
6. Hall, D.K.; Kimball, J.S.; Larson, R.; DiGirolamo, N.E.; Casey, K.A.; Hulley, G. Intensified Warming and Aridity Accelerate Terminal Lake Desiccation in the Great Basin of the Western United States. *Earth Space Sci.* **2023**, *10*, e2022EA002630. [CrossRef]
7. Wurtsbaugh, W.A.; Miller, C.; Null, S.E.; DeRose, R.J.; Wilcock, P.; Hahnenberger, M.; Howe, F.; Moore, J. Decline of the World’s Saline Lakes. *Nat. Geosci.* **2017**, *10*, 816–821. [CrossRef]
8. Hassibe, W.R.; Keck, W.G. *The Great Salt Lake*; General Information Product: Washington, DC, USA, 1991; p. 28.
9. Tarboton, D. *Collection of Great Salt Lake Data*; HydroShare: Arlington, MA, USA, 2023.
10. Division of Forestry, Fire & State Lands. U.D. of N.R. *Final Great Salt Lake Comprehensive Management Plan and Record of Decision*; SWCA: Phoenix, AZ, USA, 2013; p. 391.
11. Great Salt Lake Advisory Council Economic Significance of the Great Salt Lake to the State of Utah. Available online: <https://lf-public.deq.utah.gov/WebLink/DocView.aspx?id=392799&eqdocs=DWQ-2012-006864> (accessed on 15 November 2024).
12. Paul, D.S.; Manning, A.E. *Great Salt Lake Waterbird Survey Five-Year Report (1997–2001)*; Utah Division of Wildlife Resources: Salt Lake City, UT, USA, 2002; p. 64.

13. Sorensen, E.D.; Hoven, H.M.; Neill, J. Great Salt Lake Shorebirds, Their Habitats, and Food Base. In *Great Salt Lake Biology: A Terminal Lake in a Time of Change*; Springer: Berlin/Heidelberg, Germany, 2020; pp. 263–309, ISBN 3030403513.
14. Castellino, M.; Carle, R.; Lesterhuis, A.; Clay, R. *Conservation Plan for Wilson's Phalarope (Phalaropus Tricolor), Version 2.0*; Western Hemisphere Shorebird Reserve Network; Manomet Inc.: Manomet, MA, USA, 2024.
15. Matthews, M.W. A Current Review of Empirical Procedures of Remote Sensing in Inland and Near-Coastal Transitional Waters. *Int. J. Remote Sens.* **2011**, *32*, 6855–6899. [[CrossRef](#)]
16. Behrenfeld, M.J.; Falkowski, P.G. Photosynthetic Rates Derived from Satellite-Based Chlorophyll Concentration. *Limnol. Oceanogr.* **1997**, *42*, 1–20. [[CrossRef](#)]
17. Tebbs, E.J.; Remedios, J.J.; Harper, D.M. Remote Sensing of Chlorophyll-a as a Measure of Cyanobacterial Biomass in Lake Bogoria, a Hypertrophic, Saline-Alkaline, Flamingo Lake, Using Landsat ETM+. *Remote Sens. Environ.* **2013**, *135*, 92–106. [[CrossRef](#)]
18. Hansen, C.H.; Williams, G.P. Evaluating Remote Sensing Model Specification Methods for Estimating Water Quality in Optically Diverse Lakes throughout the Growing Season. *Hydrology* **2018**, *5*, 62. [[CrossRef](#)]
19. Wurtsbaugh, W.; Naftz, D.; Bradt, S. *Spatial Analyses of Trophic Linkages Between Basins in the Great Salt Lake*; Forestry, Fire & State Lands: Salt Lake City, UT, USA, 2008.
20. Hansen, C.H.; Burian, S.J.; Dennison, P.E.; Williams, G.P. Evaluating Historical Trends and Influences of Meteorological and Seasonal Climate Conditions on Lake Chlorophyll *a* Using Remote Sensing. *Lake Reserv. Manag.* **2020**, *36*, 45–63. [[CrossRef](#)]
21. Baskin, R.L. Occurrence and Spatial Distribution of Microbial Bioherms in Great Salt Lake, Utah. Ph.D. Thesis, University of Utah, Salt Lake City, UT, USA, 2014.
22. Lindsay, M.R.; Anderson, C.; Fox, N.; Scofield, G.; Allen, J.; Anderson, E.; Bueter, L.; Poudel, S.; Sutherland, K.; Munson-McGee, J.H.; et al. Microbialite Response to an Anthropogenic Salinity Gradient in Great Salt Lake, Utah. *Geobiology* **2017**, *15*, 131–145. [[CrossRef](#)] [[PubMed](#)]
23. Brothers, S.; Cobb, M.; Ramsey, R.D.; Wurtsbaugh, W.A.; Rivers, E. *A Multi-Tiered Assessment of Primary Production in Great Salt Lake*; Utah Division of Forestry, Fire, and State Lands: Salt Lake City, UT, USA, 2023; p. 49.
24. Pilati, A.; Wurtsbaugh, W.A. Importance of Zooplankton for the Persistence of a Deep Chlorophyll Layer: A Limnocorral Experiment. *Limnol. Oceanogr.* **2003**, *48*, 249–260. [[CrossRef](#)]
25. Standard Methods for the Examination of Water and Wastewater, 23rd ed.; 10200 Plankton; APHA Press: Washington, DC, USA, 2023.
26. Crawford, C.J.; Roy, D.P.; Arab, S.; Barnes, C.; Vermote, E.; Hulley, G.; Gerace, A.; Choate, M.; Engebretson, C.; Micijevic, E.; et al. The 50-Year Landsat Collection 2 Archive. *Sci. Remote Sens.* **2023**, *8*, 100103. [[CrossRef](#)]
27. Schaaf, C.; Wang, Z. MCD43A4 MODIS/Terra + Aqua BRDF/Albedo Nadir BRDF Adjusted Ref Daily L3 Global—500m V006. Available online: <https://lpdaac.usgs.gov/products/mcd43a4v006/> (accessed on 15 November 2024).
28. Vermote, E.; Wolfe, R. MOD09GA MODIS/Terra Surface Reflectance Daily L2G Global 1 km and 500 m SIN Grid V006. Available online: <https://lpdaac.usgs.gov/products/mod09gav006/> (accessed on 15 November 2024).
29. Gorelick, N.; Hancher, M.; Dixon, M.; Ilyushchenko, S.; Thau, D.; Moore, R. Google Earth Engine: Planetary-Scale Geospatial Analysis for Everyone. *Remote Sens. Environ.* **2017**, *202*, 18–27. [[CrossRef](#)]
30. Jakovljević, G.; Govđedarica, M.; Álvarez-Taboada, F. Waterbody Mapping: A Comparison of Remotely Sensed and GIS Open Data Sources. *Int. J. Remote Sens.* **2019**, *40*, 2936–2964. [[CrossRef](#)]
31. Belovsky, G.E.; Stephens, D.; Perschon, C.; Birdsey, P.; Paul, D.; Naftz, D.; Baskin, R.; Larson, C.; Mellison, C.; Luft, J.; et al. The Great Salt Lake Ecosystem (Utah, USA): Long Term Data and a Structural Equation Approach. *Ecosphere* **2011**, *2*, art33. [[CrossRef](#)]
32. Brivio, P.A.; Giardino, C.; Zilioli, E. Determination of Chlorophyll Concentration Changes in Lake Garda Using an Image-Based Radiative Transfer Code for Landsat TM Images. *Int. J. Remote Sens.* **2001**, *22*, 487–502. [[CrossRef](#)]
33. Han, L.; Jordan, K.J. Estimating and Mapping Chlorophyll-*a* Concentration in Pensacola Bay, Florida Using Landsat ETM+ Data. *Int. J. Remote Sens.* **2005**, *26*, 5245–5254. [[CrossRef](#)]
34. Smith, B.; Pahlevan, N.; Schalles, J.; Ruberg, S.; Errera, R.; Ma, R.; Giardino, C.; Bresciani, M.; Barbosa, C.; Moore, T.; et al. A Chlorophyll-*a* Algorithm for Landsat-8 Based on Mixture Density Networks. *Front. Remote Sens.* **2021**, *1*, 623678. [[CrossRef](#)]
35. Wang, L.; Xu, M.; Liu, Y.; Liu, H.; Beck, R.; Reif, M.; Emery, E.; Young, J.; Wu, Q. Mapping Freshwater Chlorophyll-*a* Concentrations at a Regional Scale Integrating Multi-Sensor Satellite Observations with Google Earth Engine. *Remote Sens.* **2020**, *12*, 3278. [[CrossRef](#)]
36. Markogianni, V.; Kalivas, D.; Petropoulos, G.P.; Dimitriou, E. Estimating Chlorophyll-*a* of Inland Water Bodies in Greece Based on Landsat Data. *Remote Sens.* **2020**, *12*, 2087. [[CrossRef](#)]
37. Buma, W.G.; Lee, S.-I. Evaluation of Sentinel-2 and Landsat 8 Images for Estimating Chlorophyll-*a* Concentrations in Lake Chad, Africa. *Remote Sens.* **2020**, *12*, 2437. [[CrossRef](#)]
38. Xing, X.-G.; Zhao, D.-Z.; Liu, Y.-G.; Yang, J.-H.; Xiu, P.; Wang, L. An Overview of Remote Sensing of Chlorophyll Fluorescence. *Ocean Sci. J.* **2007**, *42*, 49–59. [[CrossRef](#)]
39. Kutser, T.; Pierson, D.C.; Kallio, K.Y.; Reinart, A.; Sobek, S. Mapping Lake CDOM by Satellite Remote Sensing. *Remote Sens. Environ.* **2005**, *94*, 535–540. [[CrossRef](#)]

40. Wurtsbaugh, W.A.; Marcarelli, A.M.; Boyer, G.L. *Eutrophication and Metal Concentrations in Three Bays of the Great Salt Lake (USA)*; Watershed Sciences Faculty Publications: Salt Lake City, UT, USA, 2012; p. 70.
41. Baxter, B.K.; Litchfield, C.D.; Sowers, K.; Griffith, J.D.; Dassarma, P.A.; Dassarma, S. Microbial Diversity of Great Salt Lake. In *Adaptation to Life at High Salt Concentrations in Archaea, Bacteria, and Eukarya*; Springer: Berlin/Heidelberg, Germany, 2005; pp. 9–25.
42. Wurtsbaugh, W.A. The Great Salt Lake Ecosystem (Utah, USA): Long Term Data and a Structural Equation Approach: Comment. *Ecosphere* **2014**, *5*, 1–8. [CrossRef]
43. Wurtsbaugh, W.A. Food-Web Modification by an Invertebrate Predator in the Great Salt Lake (USA). *Oecologia* **1992**, *89*, 168–175. [CrossRef] [PubMed]
44. Great Salt Lake Ecosystem Program Algae: A Contributing Factor to the Lake’s Color (and Smell). Available online: <https://wildlife.utah.gov/gslep/wildlife/algae.html> (accessed on 15 November 2024).
45. Adams, H.; Ye, J.; Persaud, B.D.; Slowinski, S.; Kheyrollah Pour, H.; Van Cappellen, P. Rates and Timing of Chlorophyll-*a* Increases and Related Environmental Variables in Global Temperate and Cold-Temperate Lakes. *Earth Syst. Sci. Data* **2022**, *14*, 5139–5156. [CrossRef]
46. Deng, J.; Chen, F.; Hu, W.; Lu, X.; Xu, B.; Hamilton, D.P. Variations in the Distribution of Chl-a and Simulation Using a Multiple Regression Model. *Int. J. Environ. Res. Public Health* **2019**, *16*, 4553. [CrossRef] [PubMed]
47. Spall, R.E. A Hydrodynamic Model of the Circulation within the South Arm of the Great Salt Lake. *Int. J. Model. Simul.* **2009**, *29*, 181–190. [CrossRef]
48. Crosman, E.T.; Horel, J.D. MODIS-Derived Surface Temperature of the Great Salt Lake. *Remote Sens. Environ.* **2009**, *113*, 73–81. [CrossRef]
49. Lyngsgaard, M.M.; Markager, S.; Richardson, K.; Møller, E.F.; Jakobsen, H.H. How Well Does Chlorophyll Explain the Seasonal Variation in Phytoplankton Activity? *Estuaries Coasts* **2017**, *40*, 1263–1275. [CrossRef]
50. Rae, R.; Vincent, W.F. Phytoplankton Production in Subarctic Lake and River Ecosystems: Development of a Photosynthesis-Temperature-Irradiance Model. *J. Plankton Res.* **1998**, *20*, 1293–1312. [CrossRef]
51. Stephens, D.W.; Gillespie, D.M. Phytoplankton Production in the Great Salt Lake, Utah, and a Laboratory Study of Algal Response to Enrichment1: Production in Great Salt Lake. *Limnol. Oceanogr.* **1976**, *21*, 74–87. [CrossRef]
52. Wurtsbaugh, W.A. Iron, Molybdenum and Phosphorus Limitation of N2 Fixation Maintains Nitrogen Deficiency of Plankton in the Great Salt Lake Drainage (Utah, USA). *SIL Proc. 1922–2010* **1988**, *23*, 121–130. [CrossRef]
53. Marcarelli, A.M.; Wurtsbaugh, W.A.; Griset, O. Salinity Controls Phytoplankton Response to Nutrient Enrichment in the Great Salt Lake, Utah, USA. *Can. J. Fish. Aquat. Sci.* **2006**, *63*, 2236–2248. [CrossRef]
54. Ogata, E.M.; Wurtsbaugh, W.A.; Smith, T.N.; Durham, S.L. Bioassay Analysis of Nutrient and Artemia Franciscana Effects on Trophic Interactions in the Great Salt Lake, USA. *Hydrobiologia* **2017**, *788*, 1–16. [CrossRef]
55. Wurtsbaugh, W.A.; Epstein, D. Impact of the Farmington Bay Eutrophication Plume on the Plankton Ecology of Gilbert Bay, Great Salt Lake. In *Aquatic Ecology Practicum Class Report*; College of Natural Resources, Utah State University: Logan, UT, USA, 2011; Volume 41.
56. Carlson, R.E. A Trophic State Index for Lakes1. *Limnol. Oceanogr.* **1977**, *22*, 361–369. [CrossRef]
57. Wurtsbaugh, W.A.; Gliwicz, Z.M. Limnological Control of Brine Shrimp Population Dynamics and Cyst Production in the Great Salt Lake, Utah. In *Saline Lakes*; Melack, J.M., Jellison, R., Herbst, D.B., Eds.; Springer: Dordrecht, The Netherlands, 2001; pp. 119–132, ISBN 978-90-481-5995-6.
58. Fontana, C.G.; Maybruck, V.G.; Billings, R.M.; Mansfeldt, C.B.; Trower, E.J. Modeling the Microbiome of Utah’s Great Salt Lake: A Regression Analysis of Key Abiotic Factors Impacting Growth of *Dunaliella* Green Algae in the GSL’s South Arm. *bioRxiv* **2024**. [CrossRef]
59. Leavitt, P.R.; Bunting, L.; Moser, K.; Woodward, C. *Effects of Wastewater Influx and Hydrologic Modification on Algal Production in the Great Salt Lake of Utah, USA*; The University of Queensland: Brisbane, Australia, 2012.
60. Gunnell, N.; Nelson, S.; Rushforth, S.; Rey, K.; Hudson, S.M.; Carling, G.; Miller, T.; Meyers, L.; Engstrom, D. From Hypersaline to Fresh-Brackish: Documenting the Impacts of Human Intervention on a Natural Water Body from Cores, Farmington Bay, UT, USA. *Water Air Soil Pollut.* **2022**, *233*, 35. [CrossRef]
61. Byrne, A.; Tebbs, E.J.; Njoroge, P.; Nkwabi, A.; Chadwick, M.A.; Freeman, R.; Harper, D.; Norris, K. Productivity Declines Threaten East African Soda Lakes and the Iconic Lesser Flamingo. *Curr. Biol.* **2024**, *34*, 1786–1793.e4. [CrossRef]
62. King, L.; Devey, M.; Leavitt, P.R.; Power, M.J.; Brothers, S.; Brahney, J. Anthropogenic Forcing Leads to an Abrupt Shift to Phytoplankton Dominance in a Shallow Eutrophic Lake. *Freshw. Biol.* **2024**, *69*, 335–350. [CrossRef]
63. Wurtsbaugh, W.A.; Berry, T.S. Cascading Effects of Decreased Salinity on the Plankton Chemistry, and Physics of the Great Salt Lake (Utah). *Can. J. Fish. Aquat. Sci.* **1990**, *47*, 100–109. [CrossRef]
64. Maszczyk, P.; Wurtsbaugh, W.A. Brine Shrimp Grazing and Fecal Production Increase Sedimentation to the Deep Brine Layer (Monimolimnion) of Great Salt Lake, Utah. *Hydrobiologia* **2017**, *802*, 7–22. [CrossRef]

65. Jellison, R.; Melack, J.M. Algal Photosynthetic Activity and Its Response to Meromixis in Hypersaline Mono Lake, California. *Limnol. Oceanogr.* **1993**, *38*, 818–837. [[CrossRef](#)]
66. Wurtsbaugh, W.A.; Paerl, H.W.; Dodds, W.K. Nutrients, Eutrophication and Harmful Algal Blooms along the Freshwater to Marine Continuum. *WIREs Water* **2019**, *6*, e1373. [[CrossRef](#)]
67. Conover, M.R.; Bell, M.E. Importance of Great Salt Lake to Pelagic Birds: Eared Grebes, Phalaropes, Gulls, Ducks, and White Pelicans. In *Great Salt Lake Biology*; Baxter, B.K., Butler, J.K., Eds.; Springer International Publishing: Cham, Switzerland, 2020; pp. 239–262, ISBN 978-3-030-40351-5.
68. Marden, B.; Brown, P.; Bosteels, T. Great Salt Lake Artemia: Ecosystem Functions and Services with a Global Reach. In *Great Salt Lake Biology*; Baxter, B.K., Butler, J.K., Eds.; Springer International Publishing: Cham, Switzerland, 2020; pp. 175–237, ISBN 978-3-030-40351-5.
69. Richards, D.C. Nutrient Atmospheric Deposition on Utah Lake and Great Salt Lake Locations 2020, Including Effects of Sampler Type Statistical Analyses and Results. Ph.D. Thesis, Brigham Young University, Provo, UT, USA, 2021.
70. Armstrong, T.; Wurtsbaugh, W.A. *Impacts of Eutrophication on Benthic Invertebrates & Fish Prey of Birds in Farmington and Bear River Bays of Great Salt Lake*; Utah State University: Logan, UT, USA, 2019; p. 41.

**Disclaimer/Publisher’s Note:** The statements, opinions and data contained in all publications are solely those of the individual author(s) and contributor(s) and not of MDPI and/or the editor(s). MDPI and/or the editor(s) disclaim responsibility for any injury to people or property resulting from any ideas, methods, instructions or products referred to in the content.